Appl Phys A (2011) 103: 659–663
DOI 10.1007/s00339-010-6199-6

Applied Physics A
Materials Science & Processing

Photoconductivity studies on amorphous and crystalline TiO_2 films doped with gold nanoparticles

G. Valverde-Aguilar · J.A. García-Macedo · V. Rentería-Tapia · M. Aguilar-Franco

Received: 8 January 2010 / Accepted: 3 December 2010 / Published online: 4 January 2011

Abstract In this work, amorphous and crystalline TiO_2 films were synthesized by the sol–gel process at room temperature. The TiO_2 films were doped with gold nanoparticles. The films were spin-coated on glass wafers. The crystalline samples were annealed at 100°C for 30 minutes and sintered at 520°C for 2 h. All films were characterized using X-ray diffraction, transmission electronic microscopy and UV-Vis absorption spectroscopy. Two crystalline phases, anatase and rutile, were formed in the matrix TiO_2 and TiO_2/Au. An absorption peak was located at 570 nm (amorphous) and 645 nm (anatase). Photoconductivity studies were performed on these films. The experimental data were fitted with straight lines at darkness and under illumination at 515 nm and 645 nm. This indicates an ohmic behavior. Crystalline TiO_2/Au films are more photoconductive than the amorphous ones.

1 Introduction

Titanium dioxide (TiO_2) is a non-toxic material. TiO_2 thin films exhibit high stability in aqueous solutions and no photocorrosion under band gap illumination. Due to its wide-ranging chemical and physical properties (electrical conductivity, photosensitivity, and aqueous environments) TiO_2 has a large variety of potential applications. These films are already widely used in the study of the photocatalysis and photoelectrocatalysis of organic pollutants, due to its photostability and low cost [1, 2]. TiO_2 is the subject of intensive research, especially with regard to its end uses in solar cells, chemical sensors, photoelectrochemical cells and electronic devices [3, 4]. By applying a small bias, recombination of generated electron–hole pairs is retarded. As a wide band gap semiconductor, TiO_2 shows a diverse heterogeneity of crystalline phases, whereby it is possible to find it in anatase, rutile or brookite form [5].

Recently, we have observed sufficiently large photocurrents for Au–TiO_2 nanocomposites by employing appropriate electron donor. If the Au nanoparticles are embedded in a TiO_2 film, an electrode coated with the film exhibits photocurrents in an electrolyte, responding to visible light. The Au nanoparticles are photo-excited due to plasmon resonance, and charge separation is accomplished by transfer of photo-excited electrons from the Au nanoparticles to TiO_2 conduction band, and simultaneous transfer of compensative electrons from a donor in the solution to the Au nanoparticles [6]. The contact of Au and TiO_2 constructs a metal–semiconductor Schottky junction, which possibly facilitates the charge separation. The plasmon-induced charge separation is currently being exploited for a variety of applications including photovoltaic cells, visible light-responsive photocatalysis and surface patterning.

In the present work, we described the synthesis, characterization and photoconductivity behavior of amorphous and crystalline TiO_2 films doped with gold nanoparticles (NP's). The films were produced by the sol–gel process at room temperature. For amorphous films, the $HAuCl_4$ ions

G. Valverde-Aguilar (✉) · J.A. García-Macedo
Departamento de Estado Sólido, Instituto de Física, Universidad Nacional Autónoma de México, México D.F., C.P. 04510, Mexico
e-mail: valverde@fisica.unam.mx
Fax: +52-55-56225011

V. Rentería-Tapia
Departamento de Ciencias Naturales y Exactas, Universidad de Guadalajara, Centro Universitario de los Valles, C.P. 46600 Ameca, Jalisco, Mexico

M. Aguilar-Franco
Departamento de Física Química, Instituto de Física, Universidad Nacional Autónoma de México, México D.F., C.P. 04510, Mexico

were reduced by daylight and for crystalline films they were reduced by a calcination process. The obtained films were studied by X-ray diffraction (XRD), optical absorption (OA) and transmission electron microscopy (TEM). Photoconductivity studies were performed on these films to determine their transport mechanisms. Gans theory including a variable refractive index was used to fit the experimental absorption spectrum and these results are discussed.

2 Experimental

2.1 Preparation of TiO_2 solution

All reagents were Aldrich grade. The precursor solutions for TiO_2 films were prepared by the following method. Tetrabutyl orthotitanate and diethanolamine ($NH(C_2H_4OH)_2$), which prevent the precipitation of oxides and stabilize the solutions were dissolved in ethanol. After stirring vigorously 2 h at room temperature, a mixed solution of deionized water and ethanol was added dropwise slowly to the above solution with a pipette under stirring. Finally, tetraethyleneglycol (TEG) was added to the above solution. This solution was stirred vigorously to obtain a uniform sol. The resultant alkoxide solution was kept standing at room temperature to perform hydrolysis reaction for 2 h, resulting in the TiO_2 sol.

2.2 Preparation of Au stock solution

0.03 M of hydrogen tetrachloroaurate(III) hydrate ($HAuCl_4$·aq) was dissolved in a mixture of deionized water and ethanol. It was stirred for 5 minutes.

The Au stock solution was added to 20 ml of TiO_2 solution. This final solution was stirred for 17 hours at room temperature to obtain a purple color. The final chemical composition of all reagents was $Ti(OC_4H_9)_4$: $NH(C_2H_4OH)_2$: C_2H_5OH : DI H_2O : TEG : nitric acid : $HAuCl_4 = 1 : 1 : 14.1 : 1 : 1.028 : 0.136 : 0.024$. The TiO_2/Au solution has a pH = 6.0. The TiO_2 films were deposited by the spin-coating technique. The precursor solution was placed on the glass wafers (2.5×2.5 cm^2) using a dropper and spun at a rate of 3000 rpm for 20 s to produce amorphous TiO_2 film with gold ions. After that, the film was dried at 100°C for 30 min in a muffle oven in order to remove organic components and sintered at 520°C, 600°C and 700°C for 2 h in a muffle oven to produce the crystallization of the TiO_2 film with gold metallic nanoparticles.

UV-vis absorption spectra were obtained on a Thermo Spectronic Genesys 2 spectrophotometer with an accuracy of ±1 nm over the wavelength range of 300–900 nm. The structure of the final films was characterized by XRD patterns. These patterns were recorded on a Bruker AXS D8 Advance diffractometer using Ni-filtered CuKα radiation. A step-scanning mode with a step of 0.02° in the range from 1.5 to 60° in 2θ and an integration time of 2 s was used. For photoconductivity studies [7] silver electrodes were painted on the sample. It was maintained in a 10^{-5} Torr vacuum cryostat at room temperature in order to avoid humidity. For photocurrent measurements, the films were illuminated with light from an Oriel Xe lamp passed through a 0.25 m Spex monochromator. Currents were measured with a 642 Keithley electrometer connected in series with the voltage power supply. The applied electrostatic field E was parallel to the film. Light intensity was measured at the sample position with a Spectra Physics 404 power meter.

3 Results and discussion

3.1 X-ray diffraction patterns

Figure 1 shows the XRD patterns of the amorphous and crystalline TiO_2/Au films.

From the amorphous film, there is no sign of any crystal structure, which means that the TiO_2/Au film is predominantly amorphous [8]. Its spectrum only reveals the presence of gold particles by the diffraction peaks located at $2\theta = 38.24$, 44.39, 64.62 and 77.60, which can be indexed as (111), (200), (220) and (311), respectively. The position of the diffraction peaks is in good agreement with those given in ASTM data card (#04-0784).

The crystalline films sintered at different temperatures (520°C, 600°C and 700°C for 2 h) exhibit very good crystallization that corresponds to the formation of the anatase and rutile phases. In the spectrum for the crystalline film sintered at 520°C, the anatase phase was identified by the diffraction peaks located at $2\theta = 25.33$, 47.97, 54.00, 55.16 and 62.71, which can be indexed as (101), (200), (105), (211) and (204), respectively. The rutile phase was identified by the diffraction peaks located at $2\theta = 27.47$, 36.14 and 41.32, which can be indexed as (110), (101) and (111), respectively. The position of the diffraction peaks in the film is in good agreement with those given in ASTM data card (#21-1272)

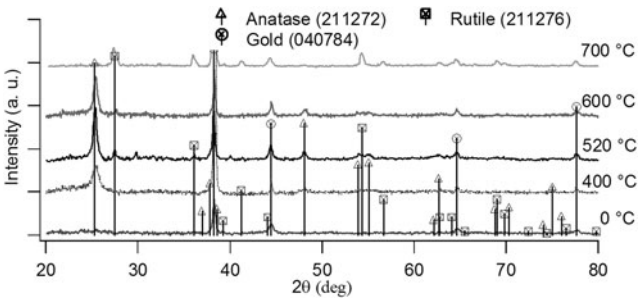

Fig. 1 XRD pattern at high angle of the amorphous and crystalline TiO_2/Au films

Table 1 Summary of nanoscopic characteristics of amorphous and crystalline TiO_2/Au films

	Phase			
	520°C *D* (nm)	600°C *D* (nm)	700°C *D* (nm)	Crystal phase (wt%) for 520°C
Anatase (101)	18.5	17.4	26.2	59.70 ± 4
Rutile (110)	26.3	23.4	14.1	37.4 ± 3
Au	–	–	–	2.90 ± 4

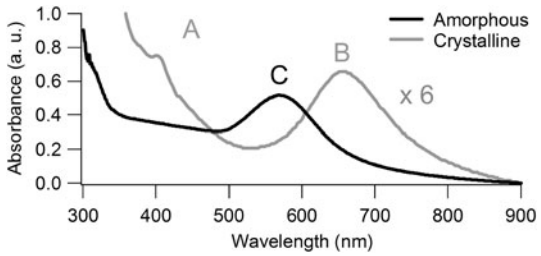

Fig. 2 OA spectra of the amorphous (*black solid line*) and crystalline (*grey solid line*) TiO_2/Au films

for anatase and ASTM data card (#21-1276) for rutile. The presence of gold NP's was detected by the same diffraction peaks identified in the amorphous film. Spectra measured at 520°C and 600°C are similar. The percentage of anatase, rutile and gold phases detected in the film sintered at 520°C was calculated by means of a Rietveld refinement (Table 1). It shows than anatase phase is bigger than rutile phase. At 700°C, the intensity of the peaks for rutile phase is more intense than that from peaks of anatase phase. It indicates that the rutile phase is the dominant species in the TiO_2 matrix.

The average crystalline size (D) was calculated from Scherrer's formula [9] by using the diffraction peak (101) for anatase phase and the peak (110) for rutile phase with $\lambda = 1.54056 \times 10^{-10}$ m. These calculations are shown in Table 1. The average grain sizes in both phases decrease when the temperature increases.

3.2 Optical absorption

Figure 2 shows the OA spectra of the amorphous and crystalline TiO_2/Au films taken at room temperature in the range of 300–900 nm. The spectrum of the crystalline film sintered at 520°C shows an absorption band A located at 402 (3.08 eV) corresponding to the TiO_2 matrix, and a second band B located 651 nm (1.93 eV) corresponding to the surface plasmon resonance (SPR) of the gold NP's. The spectrum from amorphous film shows a peak C at 568 nm (2.68 eV), which is the SPR band due to spherical Au nanoparticles [10].

To clarify the XRD and optical absorption experimental results, the formation mechanism of Au nanoparticles is

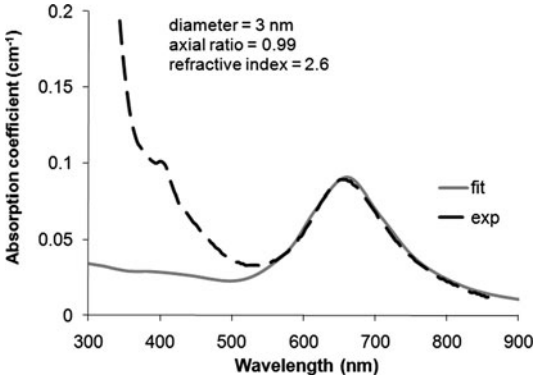

Fig. 3 OA spectrum (*black dotted line*) of the crystalline TiO_2/Au film. The calculated optical absorption spectrum (*grey solid line*) was obtained by Gans theory

discussed below. It is known that the photolysis of $HAuCl_4$ to the Au atom, Au^0, is a multiphoton event [11], and it proceeds by irradiation. Therefore, for amorphous TiO_2/Au film, the Au nucleation was slow and random because the $HAuCl_4$ ions were reduced by daylight (containing a little UV light) and this mostly happened after the gelation. The nuclei were thus distributed randomly within the TiO_2 skeleton and consequently led to the growth of the Au particles that were inhomogeneous, and their size distribution was very wide.

Literature [7, 12] reports an absorption peak for surface plasmon resonance (SPR) of gold nanoparticles around 500–550 nm. A red-shift in the maximum in absorbance toward larger wavelength (from 568 to 651 nm) with respect to the amorphous TiO_2 film is evident as well as a broadening of the peak absorption width compared to the amorphous film. The dependence of this shift on the embedding medium indicates the high sensitivity of surface plasmon band to cluster-matrix interface properties. This fact originates with the increase in the diameter of Au nanoparticles and an increment of the refractive index of TiO_2 matrix with increasing heat-treatment temperature [13]. It is well known that the refractive index of TiO_2 films is related to the crystal phase (anatase or rutile), the crystalline size and the densities of the films [14]. For these reasons, the OA spectrum (Fig. 2) of the crystalline film was fitted very well using Gans theory [15] with a local refractive index $n_{\text{local}} = 2.6$ (Fig. 3). This index has a value close to the refractive index reported for the anatase phase ($n_{\text{anatase}} = 2.54$) [16]. This is consistent with the result of XRD which indicates that the anatase phase has the highest proportion (59.7 wt%). The rutile phase ($n_{\text{rutile}} = 2.75$) also contributes to this high refractive index in a minor proportion (37.4 wt%).

3.3 HRTEM measurements

Figure 4 shows the HRTEM images of the crystalline TiO_2/Au film sintered at 520°C. Figure 4(a) shows gold

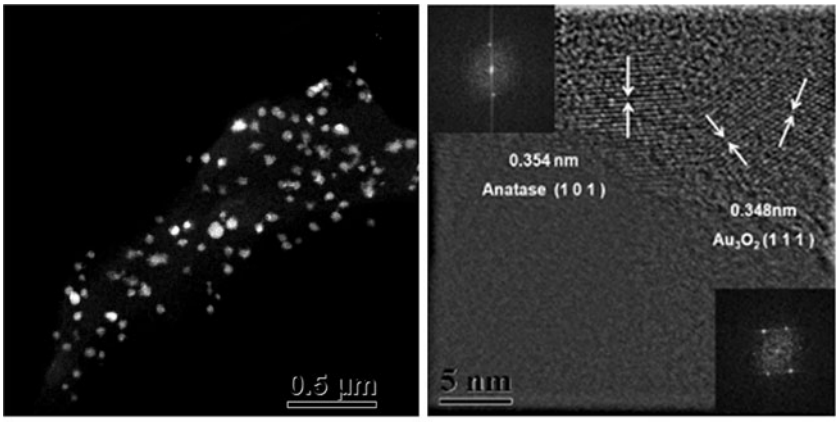

Fig. 4 (**a**) HRTEM image of the crystalline TiO_2/Au film exhibits several gold NP's. (**b**) The reflections corresponding to anatase nanocrystals and gold nanoparticles are identified with *white arrows*

NP's which were identified as brilliant particles. Figure 4(b) shows the reflection (101), which corresponds to the anatase phase; and the reflection (111) corresponds to the gold nanoparticle identified as Au_3O_2. The inset shows the diffraction patterns showing these reflections. From HRTEM studies taking into account a population of gold NP's, the corresponding size-distribution histograms were obtained. The distributions from the major axis A and minor length axis B and their respective standard deviations are $A = 9.8 \pm 7.8$ nm and $B = 6.6 \pm 3.9$ nm, respectively.

3.4 Photoconductivity studies

Usually [7] Ohm's law under light illumination is given by

$$\vec{J} = \vec{J}_{ph} + (\sigma_d + \sigma_{ph})\vec{E} \tag{1}$$

where $\vec{J}_{ph}$ is the photovoltaic current density and σ_{ph} is the photoconductivity. When the current densities are assumed to be parallel to the electric field $\vec{E}$ equation (1) becomes the following one:

$$J = \frac{e\phi l_0 \alpha I}{h\nu} + \left(\sigma_d + \frac{e\phi\mu\tau\alpha I}{h\nu}\right)E \tag{2}$$

with ϕ as the quantum efficiency of charge carrier photogeneration, l_0 as the charge carrier mean free path, α as the sample absorption coefficient, I as the light intensity at the frequency ν of illumination, h as the Planck's constant and τ as the charge carriers mean lifetime. The first term is the photovoltaic transport effect, the second one is the dark conductivity $\sigma_d = en_0\mu$ (n_0 is the carrier density that produces dark conductivity and μ is the charge mobility), and the third one is the photoconductivity itself.

Equation (2) can be written as

$$J = A_1 E + J_0 \tag{3}$$

From the absorption spectrum of crystalline film sintered at 520°C (Fig. 2), the illumination wavelength for photoconductivity studies was chosen: 645 nm that corresponds to the maximum absorption band and 515 nm were there is no absorption. Photoconductivity results of amorphous and crystalline TiO_2 films with gold NP's are shown in Fig. 5. Current density as function of electric applied field on the film was plotted. The experimental data were fitted by least-squares with straight lines at darkness and under illumination. This indicates an ohmic behavior. The linear fits are shown in Table 2.

Table 2 Linear fittings of amorphous and crystalline TiO_2 films

λ (nm)	TiO_2/Au film	A_1	J_0
645	Crystalline	3.14×10^{7}	1.40×10^{-3}
	Amorphous	5.36×10^{-10}	2.89×10^{-6}
515	Crystalline	3.64×10^{-7}	1.07×10^{-3}
	Amorphous	4.97×10^{-10}	2.27×10^{-6}
Darkness	Crystalline	3.73×10^{-7}	6.66×10^{-4}
	Amorphous	3.32×10^{-10}	1.89×10^{-6}

For both kinds of TiO_2/Au films, when the illumination wavelength decreases the J_0 value decreases. For a crystalline film, when the illumination wavelength decreases, the slope A_1 increases. It indicates a strong photoconductive behavior in these films. It is in accordance to the fact that the gold nanoparticles have sizes of ∼9.8 nm, which leads a better conduction of the carriers [6].

4 Conclusions

High optical quality crystalline TiO_2 films with gold NP's were obtained by sol–gel process. XRD measurements reveal the presence of the anatase and rutile phases, which were produced after sintering treatments. For rutile phase, the crystallite size decreases when the temperature increases from 520°C to 700°C.

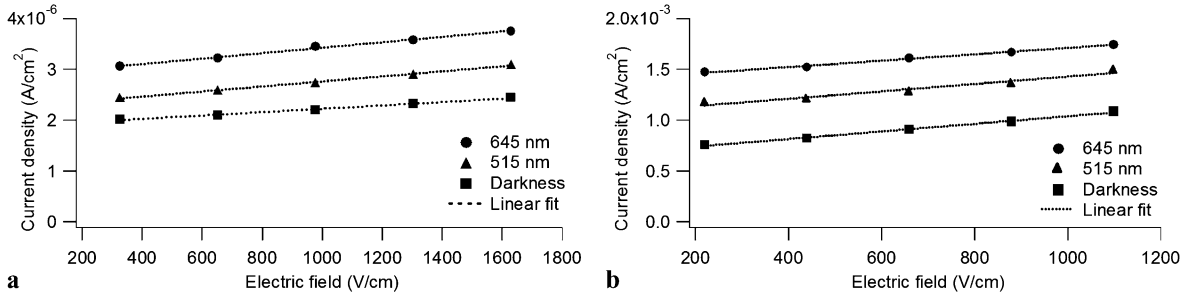

Fig. 5 Plots of current density vs. electric field spectra for (**a**) amorphous and (**b**) crystalline TiO_2/Au films. Linear fits correspond to the *dotted lines*

For film sintered at 520°C, the anatase phase has a bigger proportion (59.75 wt%) than the rutile phase (37.4 wt%). The optical absorption spectrum was very well fitted using Gans theory considering a local refractive index $n_{\text{local}} = 2.6$. This index is related to refractive index from crystal phases, anatase and rutile, taking into account that the anatase is the major phase. The experimental data J vs. E were fitted by straight lines corresponding to an ohmic behavior. Crystalline TiO_2/Au films exhibit a strong photoconductive effect. Anatase phase leads a better conduction of the carriers than the amorphous phase.

Acknowledgements The authors acknowledge the financial supports of CONACYT 79781, NSF-CONACYT, PUNTA, ICYTDF, Red NyN and PAPIIT IN107510. GVA is grateful for CONACyT fellowship. The authors are thankful to Luis Rendón (HRTEM), Roberto Hernández-Reyes (SEM) and Diego Quiterio (preparation of the samples for SEM studies) for technical assistance.

References

1. M. Addamo, V. Augugliaro, A. Di Paola, E. García-López, V. Loddo, G. Marcì, R. Molinari, L. Palmisano, M. Schiavello, Preparation, characterization, and photoactivity of polycrystalline nanostructured TiO_2 catalysts. J. Phys. Chem. B **108**, 3303–3310 (2004)
2. Y. Shaogui, Q. Xie, L. Xinyong, L. Yazi, C. Shuo, C. Guohua, Preparation, characterization and photoelectrocatalytic properties of nanocrystalline Fe_2O_3/TiO_2, ZnO/TiO_2, and Fe_2O_3/ZnO/TiO_2 composite film electrodes towards pentachlorophenol degradation. Phys. Chem. Chem. Phys. **6**(3), 659–664 (2004)
3. C. Graziani Garcia, N.-Y. Murakami Iha, R. Argazzi, C.-A. Bignozzi, 4-Phenylpyridine as ancillary ligand in ruthenium (II) polypyridyl complexes for sensitization of n-type TiO_2 electrodes. J. Photochem. Photobiol. A **115**(3), 239–242 (1998)
4. S. Dueñas, H. Castán, H. García, E. San Andrés, M. Toledano-Luque, I. Mártil, G. González-Díaz, K. Kukli, T. Uustare, J. Aarik, A comparative study of the electrical properties of TiO_2 films grown by high-pressure reactive sputtering and atomic layer deposition. Semicond. Sci. Technol. **20**(10), 1044–1051 (2005)
5. L. Hu, T. Yoko, H. Kosuka, S. Sakka, Effects of solvent on properties of sol-gel derived TiO_2 coating films. Thin Solid Films **219**(1–2), 18–23 (1992)
6. K. Yu, Y. Tianw, T. Tatsuma, Size effects of gold nanaoparticles on plasmon-induced photocurrents of gold–TiO_2 nanocomposites. Phys. Chem. Chem. Phys. **8**, 5417–5420 (2006)
7. J. García M., G. Valverde, D. Cruz, A. Franco, J.I. Zink, P. Minoofar, Structure and PPV concentration effect on the photoconductivity response from mesostructured silica films. J. Phys. Chem. B **107**(10), 2249–2252 (2003)
8. A.E. Jiménez González, S. Gelover Santiago, Structural and optoelectronic characterization of TiO_2 films prepared using the sol–gel technique. Semicond. Sci. Technol. **22**, 709–716 (2007)
9. G.J. Wilson, A.S. Matijasevich, D.R.G. Mitchell, J.C. Schulz, G.D. Will, Modification of TiO_2 for enhanced surface properties: finite Ostwald ripening by a microwave hydrothermal process. Langmuir **22**(5), 2016–2027 (2006)
10. M.G. Manera, J. Spadavecchia, D. Busoc, C. de Julián Fernández, G. Mattei, A. Martucci, P. Mulvaney, J. Pérez-Juste, R. Rella, L. Vasanelli, P. Mazzoldi, Optical gas sensing of TiO_2 and TiO_2/Au nanocomposite thin films. Sens. Actuators B **132**(1), 107–115 (2008)
11. W. Shen, F.G. Liu, J. Qiu, B. Yao, The photoinduced formation of gold nanoparticles in a mesoporous titania gel monolith. Nanotechnology **20**(10), 105605 (2009)
12. J. Yu, L. Yue, S. Liu, B. Huang, X. Zhang, Hydrothermal preparation and photocatalytic activity of mesoporous Au–TiO_2 nanocomposite microspheres. J. Colloid Interface Sci. **334**(1), 58–64 (2009)
13. A. Ito, H. Masumoto, T. Goto, Optical properties of Au nanoparticle dispersed TiO_2 films prepared by laser ablation. Mater. Trans. **44**(8), 1599–1603 (2003)
14. C.J. Brinker, G.C. Frye, A.J. Hurd, C.S. Ashley, Fundamentals of sol–gel dip coating. Thin Solid Films **201**(1), 97–108 (1991)
15. V.M. Rentería, J. García-Macedo, Influence of the local dielectric constant on modeling the optical absorption of silver nanoparticles in silica gels. Colloids Surf. A, Physicochem. Eng. Asp. **278**(1–3), 1–9 (2006)
16. Z. Wang, U. Helmersson, P.-O. Käll, Optical properties of anatase TiO_2 thin films prepared by aqueous sol–gel process at low temperature. Thin Solid Films **405**, 50–54 (2002)